THE JOURNAL OF PHYSICAL CHEMISTRY C

Article

pubs.acs.org/JPCC

Monte Carlo Simulation of Geminate Pair Recombination Dynamics in Organic Photovoltaic Devices: Multi-Exponential, Field-Dependent Kinetics and Its Interpretation

Matthew L. Jones,[†] Buddhapriya Chakrabarti,[§] and Chris Groves*,[†]

[†]School of Engineering and Computing Sciences, Durham University, South Road, DurhamDH1 3LE, United Kingdom

[§]Department of Mathematical Sciences, Durham University, South Road, Durham DH1 3LE, United Kingdom

Supporting Information

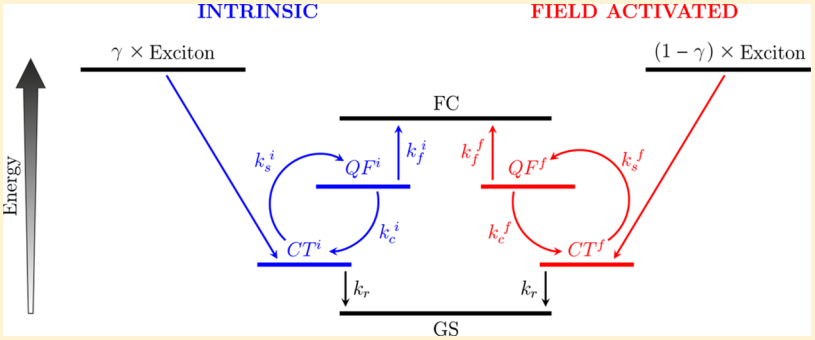

ABSTRACT: Monte Carlo simulations are used to examine charge-transfer (CT) state recombination dynamics considering the effects of energetic disorder and bulk heterojunction morphology. Strongly biexponential recombination kinetics were observed, in agreement with spectroscopy. Data over a range of electric fields $10^6 \leq F \leq 10^8$ V m^{-1} suggest that the slow component of recombination is due to energetic and spatial trapping of charges, as increasing the field reduces the magnitude of the slow decay. This behavior could not be described using a simple Onsager−Braun type model; hence, an alternative kinetic framework including an intermediate "quasi-free" state between the CT state and free charges is proposed and subsequently shown to fit the MC data very well. The predictive capability of the modified model was then tested by repeating MC simulations with an altered recombination rate. It is shown that more than just the recombination rate had to be changed in the modified kinetic model to retrieve good agreement with MC simulations. This suggests that the derived rates from the modified kinetic model do not have exact correspondence with physical processes in organic photovoltaic blends. We attribute the difficulty in fitting kinetic models to CT recombination data to the dispersive nature of hopping transport.

1. INTRODUCTION

Organic photovoltaic devices (OPVs) are an attractive alternative to their inorganic counterparts because of the capability to tune their absorption to the solar spectrum[1] and the availability of scalable manufacturing processes.[2,3] However, unlike inorganic photovoltaics, photoabsorption in OPVs results in an exciton with a large binding energy.[4] Efficient charge generation in OPVs is instead achieved using a pair of materials, the donor and acceptor, in which the highest occupied and lowest unoccupied molecular orbitals (HOMOs and LUMOs respectively) form a type-II heterojunction. This type-II heterojunction facilitates charge transfer of the hole from the exciton to the donor HOMO or the electron from the exciton to the acceptor LUMO. The resulting charge-transfer (CT) state can either recombine geminately to the ground state (GS) or further separate into free charges (FC), which can in turn be extracted at the electrodes as useful current. The efficiency with which CT states are converted into free charges (η) is therefore vital in determining the power conversion efficiency of OPVs.

Given the strong Coulomb attraction between charges (dielectric constant $\varepsilon \sim 3$), one may expect η to be either small or field-dependent.[5,6] While this behavior has been reported for some OPVs,[7,8] in others η has been shown to be large or field-independent.[7,9,10] The physical reasons for this diverse behavior have, and continue to be, the subject of much research.[11] Spectroscopic techniques are particularly useful to further understand the CT dissociation process, with time-resolved photoluminescence (PL) spectroscopy and photo-induced absorption (PIA) allowing examination of CT state decay and dynamics of excited state populations respectively.

Analysis of excited state dynamics measured by spectroscopy commonly involves a kinetic model in which the various excited

Received: August 12, 2013
Revised: September 24, 2013
Published: January 9, 2014

   dx.doi.org/10.1021/jp408063f | J. Phys. Chem. C 2014, 118, 85−91

states and transition rates are defined on an energy level (Jablonski) diagram. The transition rates are then fitted to reproduce the observed dynamic behavior. Perhaps the simplest kinetic model of excited state dynamics in an OPV is given by Onsager–Braun[5,6] (OB) shown in Figure 1. Here the exciton

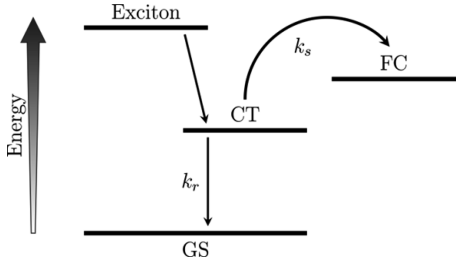

Figure 1. Schematic for the Onsager–Braun (OB) description of charge generation and separation. The rate coefficients k_s and k_r describe the separation and recombination processes respectively.

incident on the donor–acceptor interface creates a CT state which may then either recombine to the ground state with a rate k_r, or separate to free charges with a rate k_s. We note that the schematic figure in the Braun paper shows a feedback path between the free charge and CT states. However in the subsequent analysis, the equation for dissociation efficiency does not reflect this feedback path. This type of model has been successfully fitted to spectroscopy data in a range of OPV systems.[12,13] However, excited state dynamics in some OPV systems cannot be well fitted by an OB type model. In these cases the energy level diagram is modified to include the physical processes of interest, such as feedback between the FC and CT state,[14,15] ultrafast charge generation,[7,16] or decay routes via intermediate excited states[8,17] to name a few.

Because only a finite number of states can be considered in a kinetic model, energy diagrams necessarily simplify the charge separation process. A CT state must achieve a mutual separation of $r_c \sim 15–20$ nm, at which the mutual Coulomb interaction reduces to $\sim k_B T$, and the state *may* be considered converted into free charges. In the absence of charge delocalization, this will occur via a series of hops which individually may either increase or decrease separation of charges. This manifold of intermediate states is difficult to consider using a kinetic model. In turn, this leads to difficulties in understanding complex dynamic behavior as well as relating fitted rates to quantum chemical calculations of recombination or hopping rates.[18]

The degree of confidence one can have with a particular kinetic scheme is somewhat dependent on the efficiency of the OPV system. In an inefficient OPV system, transport through and trapping in intermediate states may be expected to be significant, and kinetic models will inevitably be more approximate. In efficient OPV systems, the number of hops between CT and FC states may be fewer. Charges may become effectively free at separations smaller than r_c because of the effect of energetic disorder,[19,20] the driving force of entropy,[21] or cascaded energy heterojunctions.[22,23] Furthermore, efficient OPVs may benefit from delocalization of the CT state[17,24,25] or the exciton,[26] which increases the initial separation of the charges, so reducing the distance charges have to travel before becoming free.

Nonetheless, even with these caveats, it is likely that the charges generated from CT states will have to separate by a distance of some nanometers via intermediate transport states before becoming free charges. In this paper, we examine the impact of these intermediate transport processes on CT state dynamics and the issues this causes for interpretation using kinetic models.

The paper is arranged as follows. In Monte Carlo Simulations, the dynamics and efficiency of CT state dissociation are examined using a Monte Carlo (MC) model at a variety of electric fields. This model describes charge hopping in an energetically disordered bulk heterojunction morphology but omits hot CT states; therefore, it can be considered as the most basic case of CT state dissociation. In Modified Kinetic Model, these MC data are interpreted using a kinetic model, similar to the analysis of spectroscopic data. This enables examination of the relationship between known physical processes and rates within the MC model, and the rates derived using the kinetic model. MC simulations reveal field-dependent, multiexponential recombination dynamics in agreement with experiment. It is shown that the mean recombination time is only loosely related to the recombination rate of charges, k_r. The wide range of data produced by MC, which includes separation efficiency and recombination dynamics as a function of electric field, could not be fitted with existing kinetic models. An alternative kinetic model is proposed that yields reasonable fits to all MC data; furthermore, it is shown to predict the behavior of the MC data when the recombination rate is changed. However, it is also shown that in order to achieve the fits to MC data with an altered recombination rate, the rate constants have to be altered in ways which are not representative of the MC model. This suggests the kinetic models, while useful to fit to experimental data, do not always have exact correspondence with physical processes occurring in an OPV.

2. RESULTS AND DISCUSSION

2.1. Monte Carlo Simulations. The MC model used to simulate CT state dissociation is similar to that described elsewhere.[27–29] The aim of this model is to recreate CT state dissociation in an OPV considering energetic disorder and bulk heterojunction morphology. More complex considerations such as hot CT states are omitted here but will be the subject of future investigations. We note that MC simulations of this type have been successful in obtaining quantitative agreement with all-polymer[30,31] and inefficient polymer–fullerene[20] OPVs.

The simulation volume is partitioned into a regular, 3-dimensional Cartesian grid with a lattice size of 1 nm which extends in 128 nm in each direction. The sites are assigned as donor or acceptor in accordance with a bulk heterojunction morphology generated numerically using modified Cahn–Hilliard theory.[32–34] The blend used was as reported elsewhere[32] and has a 1:1 donor–acceptor volume ratio, an optimized domain size of 7 nm, and sharp interfaces between pure donor and acceptor domains. Each site is additionally assigned a Gaussian distributed random energy to simulate the effects of energetic disorder. The standard deviation of the Gaussian distribution was chosen to be $\sigma = 0.1$ eV, which is similar to typical values for amorphous conjugated polymers.[35]

A single simulation started with the injection of an electron–hole pair (CT state) at either side of a random donor–acceptor interface. Charges were then permitted to hop to nearest neighbor cells of the appropriate material (e.g., electrons to acceptor) at a rate given by the Marcus expression[36]

dx.doi.org/10.1021/jp408063f | J. Phys. Chem. C 2014, 118, 85–91

$$k_{hop} = \nu_0 \exp\left(-\frac{(\Delta E + E_r)^2}{4E_r k_B T}\right) \quad (1)$$

where ν_0 is a hopping prefactor related to the electronic coupling between the initial and final states, k_B the Boltzmann constant, and T the absolute temperature. ΔE is the difference in energy between the origin and destination states, and E_r is the reorganization energy required. ΔE includes contributions from the internal electric field and Coulombic interactions. To produce carrier mobilities similar to those reported for charges in amorphous conjugated polymers (here $\mu = 4.2 \times 10^{-6}$ cm^2 V^{-1} s^{-1}),[28] E_r was set as 4×10^{-20} J, while $\nu_0 = 1 \times 10^{11}$ s^{-1}. The transport of electrons and holes was assumed to be the same for simplicity. This makes the implicit assumption that electronic coupling between sites is both homogeneous and time-independent. Adjacent charges recombined at a rate $k_r = 10^7$ s^{-1}, similar to that reported for all-polymer blends.[37] Waiting times for each process were generated from these rates using the following equation:

$$\tau = -\frac{\ln x}{k} \quad (2)$$

where x is a uniformly distributed random number between 0 and 1 and k is the rate in question. The shortest waiting time of the possible events was chosen as the behavior for that particle. After a hop has taken place, the Coulomb interaction is not recalculated for the opposing charge. This approximation, known as the first reaction method (FRM), reduces simulation run-time and has been shown to have little effect on the dynamic behavior of charge separation in situations very similar to those examined here (i.e., all-polymer bulk heterojunction OPVs).[28] Simulations proceeded until the charges had either recombined or separated, here defined when the charges reach a mutual separation of 25 nm. This process was repeated for at least 7×10^6 iterations over 15 configurations of energetic disorder to obtain reliable statistics.

Measuring the behavior of successive individual charge pairs implies that the observed kinetics correspond to low excitation fluence in experiment. Furthermore, we define a definite end point of our simulation whereupon geminate recombination is deemed to have not occurred. This separation between (prompt) geminate recombination and subsequent (delayed) nongeminate recombination is somewhat artificial; however, we note that at low pump fluence, the kinetics of geminate and nongeminate recombination typically occur on different time scales,[38,39] and so we argue that it is reasonable to consider geminate recombination separately from bimolecular recombination.

CT state dynamics were simulated for a range of electric fields between $10^6 \leq F \leq 10^8$ V m^{-1}, representing an OPV bias range extending from reverse bias (where collection of charges is efficient) through the operating region. The full data set is shown in Figure S1 of the Supporting Information. For each electric field, the probability density function of recombination time $P_r(t)$ and the CT state separation efficiency η were measured. The recombination dynamics recorded here (i.e., $P_r(t)$) most closely correspond to time-resolved PL measurements in experiment. However, we note that the findings of this paper are not sensitive to examining recombination dynamics because tracking the population of CT states (which we define as charge pairs with separation <2 nm) gives rise to similar behavior, as discussed in more detail later.

From these data we calculate the mean recombination time $\langle \tau_{rec} \rangle$ as

$$\langle \tau_{rec} \rangle = \int_0^{t_{max}} t P_r(t)\, dt \quad (3)$$

where t_{max} was the time at which $P_r(t)$ had dropped by 3 orders of magnitude, corresponding to the signal range available in experiment.

The symbols in Figure 2a show the MC calculated $\langle \tau_{rec} \rangle$ as a function of field. It is apparent that $\langle \tau_{rec} \rangle$ is field dependent,

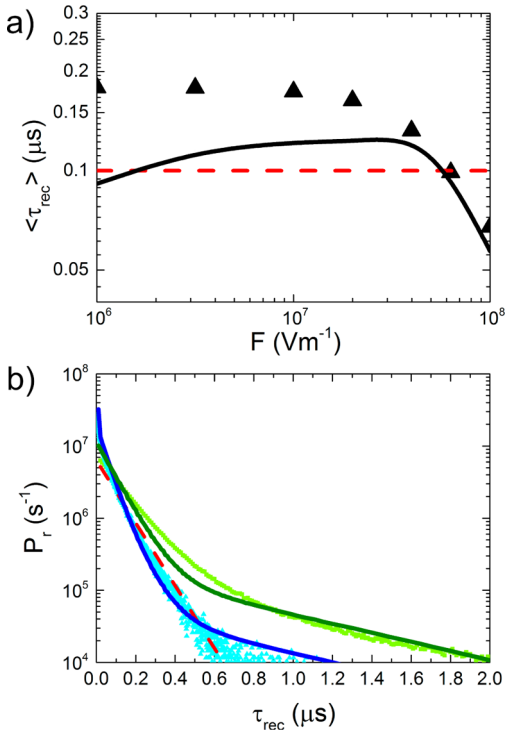

Figure 2. Recombination dynamics from Monte Carlo simulations with $k_r = 10^7$ s^{-1}. (a) $\langle \tau_{rec} \rangle$ for both the MC simulations (black triangles) and the kinetic model (black line). (b) $P_r(t)$ obtained by MC (symbols) and the kinetic model (lines) for $F = 10^6$ V m^{-1} (green) and $F = 10^8$ V m^{-1} (blue). In both panels, the red dashed lines show the inverse recombination rate k_r.

being larger than the inverse recombination rate $(1/k_r)$ at fields corresponding to the operating region of an OPV and smaller than $1/k_r$ at high fields corresponding to strong reverse bias ($F = 10^8$ V m^{-1}). This dynamic behavior is examined further in Figure 2b, which shows that $P_r(t)$ is generally biexponential, with a slow decay component with a characteristic rate smaller than $1/k_r$. This is in agreement with preliminary work by the author,[19] although here the biexponential behavior and field dependence of $P_r(t)$ are revealed more clearly because of the larger sample size. The prominence of the slow decay component is shown to increase as the field reduces (all fields examined are shown in Figure S1 of the Supporting Information). In Figure S2 of the Supporting Information, we show that the CT state population has similar field-dependent biexponential dynamics. We attribute the slow decay to energetically and morphologically trapped charges, which eventually detrap and are afforded another chance to recombine (albeit with a separation efficiency that has been modified from when the charges were first created adjacent to the donor–acceptor interface). Applying an electric field reduces the

dx.doi.org/10.1021/jp408063f | J. Phys. Chem. C 2014, 118, 85−91

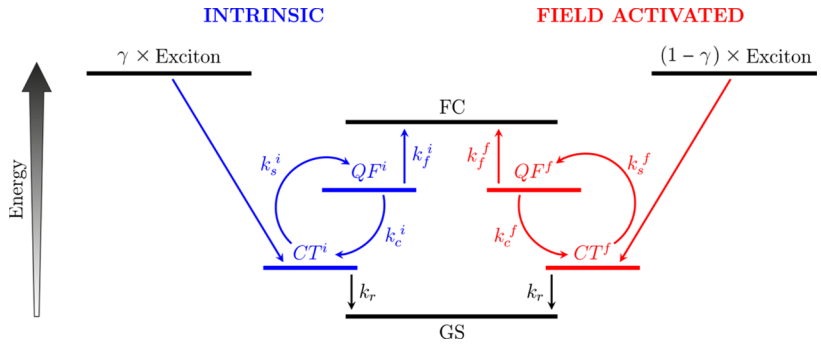

Figure 3. Schematic of the proposed kinetic scheme. Two independent populations of charges are produced (with field dependent probability γ), representing intrinsic (superscript *i*, blue) and field-activated (superscript *f*, red) recombination pathways. The rate coefficients k_s, k_c, k_f, and k_r describe separating, collapsing, freeing, and recombining processes respectively.

likelihood of trapping; hence, the prominence of the slow decay reduces. This mechanism has been reported elsewhere to explain experimental data.[40,41] The initial "fast" decay of $P_r(t)$ is reasonably well-described by $1/k_r$, however, the rate of decay is shown to increase with field. We attribute the field-dependence of the fast decay to field-dependent charge transport "emptying" the CT state and therefore reducing the potential for recombination.

Multiexponential CT state dynamics of the type shown in Figure 2b are ubiquitous throughout the literature. In many cases, bi- or triexponential decays are fitted to data, although often[8,41] the third decay component occurs on a faster time scale than the instrument response time, leaving two free parameters to describe the observable kinetics. We now move on to discuss interpretation of these types of data using kinetic models.

The simplest kinetic scheme is provided by the OB model shown in Figure 1, in which the CT state branches to either the ground state or free charges. In these circumstances, the lifetime of the CT state is described by

$$\tau_{CT} = \frac{1}{k_r + k_s} \tag{4}$$

At low fields, when $k_s \to 0$, $\tau_{CT} \to 1/k_r$. At high fields, when $k_s \gg k_r$, then $\tau_{CT} \to 1/k_s$. Hence, a simple branching model can explain $\tau_{CT} < 1/k_r$ (shown in Figure 2 at high fields), but it cannot explain $\tau_{CT} > 1/k_r$ at low field (shown in Figure 2) nor biexponential $P_r(t)$ (Figure 2b) for a single recombination rate.

Due to the inability of simple OB type models to describe biexponential kinetics and the field dependence thereof, a variety of modifications have been suggested. These include the incorporation of a manifold of CT states,[8,42] feedback via charge transport,[14,15] energetic and morphological trapping,[40,41] or multiple separation/decay pathways.[43,44] The MC simulations here include some elements of these physical processes. However, we have shown that biexponential behavior need not be due to multiple decay pathways because only one recombination rate exists in our MC model. Our aim is to now analyze the data of Figure 2, and the associated separation efficiency, with the simplest kinetic model which can satisfactorily reproduce the observed trends.

2.2. Modified Kinetic Model. Here we propose a kinetic framework to describe CT state dynamics measured using MC. Considering the MC simulation, we identify the following types of states to include on the energy diagram. As with OB, the ground state (GS) and free charges (FC) are defined as "sinks", representing the end points of recombination and successful separation, respectively. There is also a CT state, which is directly created from the exciton and from which recombination can occur. However, unlike this model we also include a manifold of states intermediate between CT and free charges, within which charges may be considered to be Coulombically bound but are not eligible to recombine. The manifold is collected into a single state which we term "quasi-free" (QF). Similar to the MC simulation, charges in the QF state can separate further into free charges, or "collapse" back to the CT state. This is conceptually similar to the work of Wojcik and Tachiya,[45] who describe nonsingle-exponential separation and modify OB mathematically by alleviating the constraint that recombination cannot occur beyond the reaction radius. However, as described in the Supporting Information, a simple scheme involving a single set of CT, GS, QF, and FC states does not adequately describe all of the Monte Carlo data (see Figure S3 of the Supporting Information and accompanying discussion). Instead, it was found that a combination of two recombination pathways, which we term intrinsic and field-activated (shown in Figure 3) could satisfactorily fit these data. The fraction of excitons which dissociate via the intrinsic route is defined as γ, meaning the fraction of excitons which dissociate via the field-activated route is $(1 - \gamma)$. The dynamic behavior of this scheme can be described by the following coupled ordinary differential equations:

$$\frac{d[CT^x]}{dt} = -k_r{}^x[CT^x] - k_s{}^x[CT^x] + k_c{}^x[QF^x] \tag{5}$$

$$\frac{d[QF^x]}{dt} = k_s{}^x[CT^x] - k_c{}^x[QF^x] - k_f{}^x[QF^x] \tag{6}$$

$$\frac{d[FC]}{dt} = k_f{}^i[QF^i] + k_f{}^f[QF^f] \tag{7}$$

$$\frac{d[GS]}{dt} = k_r[CT^i] + k_r[CT^f] \tag{8}$$

where the superscript x represents either the field-activated (f) or intrinsic (i) pathways and square brackets denote the population of each state; the rate coefficients $k_s{}^x$, $k_c{}^x$, and $k_f{}^x$ are depicted in Figure 3. The separation efficiency η is calculated by solving the differential equations for the intrinsic and field-activated pathways separately to obtain the population of the ground state at long times for each route; then the overall η is calculated by combining them in proportion using γ.

We placed the following constraints to limit the parameter space. The rate coefficients for the intrinsic pathway were

dx.doi.org/10.1021/jp408063f | J. Phys. Chem. C 2014, 118, 85−91

assumed to be constant with field, while the field-activated rate coefficients were permitted to vary linearly with electric field. We assumed that for the inefficient OPV blends examined here, intrinsic charge generation dominates at low fields (i.e., $\gamma \rightarrow 1$). As the field increases, charges can detrap and the field-activated route becomes more important (i.e., γ reduces). Hence, γ must decrease monotonically with increasing field.

A variable-time step fourth-order Runge–Kutta method was used to numerically solve the coupled differential eqs 5–8. The free parameters in these equations were fitted to η, $\langle\tau_{rec}\rangle$, and $P_r(t)$ measured by MC subject to the constraints mentioned above. These parameters are shown in Figures 4c,d. As can be seen from Figure 4a, excellent fits to η are obtained. We note that the MC prediction of η is small (<0.1) below 10^7 V m^{-1}, which corresponds approximately to the operating range of an OPV. This is because we here utilize model parameters which correspond to all-polymer (and more specifically polyfluorene[46]) OPVs, which show inefficient charge separation when compared to their polymer–fullerene counterparts. Figure 2b and Figure S1 of the Supporting Information show excellent agreement between the kinetic model and MC $P_r(t)$ over a range of fields. In particular, the field-dependence of the initial "fast" and delayed "slow" component of $P_r(t)$ are recreated faithfully. The biexponential character of $P_r(t)$ in this case arises primarily because of feedback from the QF to the CT state, which repopulates the CT state at later times and affords another (delayed) opportunity at recombination. Reasonable fits are obtained for $\langle\tau_{rec}\rangle$ also, shown in Figure 2a. As for the MC data, $\langle\tau_{rec}\rangle$ for the kinetic model was calculated as described in eq 3, where t_{max} was the time at which the kinetic model prediction of $P_r(t)$ had dropped by 3 orders of magnitude. We note that if we took $t_{max} \rightarrow \infty$, as is possible using numerical techniques, the agreement between the kinetic and MC model predicted $\langle\tau_{rec}\rangle$ is much better than that shown in Figure 2a because of a cancellation of errors in the shapes of $P_r(t)$ (Figure S4 of the Supporting Information). Figure 4b shows the monotonic decay of the parameter γ as a function of field strength, F. The separation of CT states at low fields are almost solely intrinsic, until the field-activated separation begins to dominate at $F \sim 2.5 \times 10^7$ V m^{-1}, which corresponds to the sharp increase in η shown in Figure 4a.

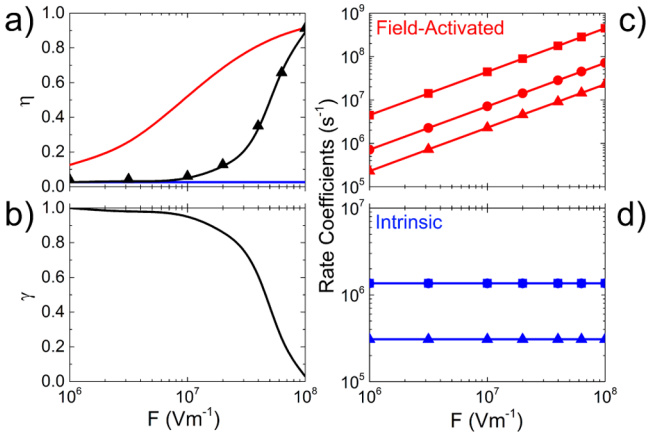

Figure 4. (a) Separation efficiencies of the field-activated (red solid line) and intrinsic (blue solid line) pathways alone and their combined efficiency (black solid line), with η from the Monte Carlo simulations, assuming $k_r = 10^7$ s^{-1} (black triangles). (b) Fraction of CT states in the intrinsic decay channel (γ) as a function of varying electric field (F). (c) and (d) show the variation of the rate coefficients k_s (squares), k_c (circles), and k_f (triangles) as a function of F, for the field-activated ((c), red) and intrinsic ((d), blue) recombination pathways. Note that $k_s^i = k_c^i$, so the two graphs are coincident.

Given that the kinetic model was fitted to a wider range of MC data than is generally available in experiment, it might be expected that the present kinetic model would be a more complete description of CT state dynamics for this simple system. Here we test the robustness of the new kinetic model by performing further MC simulations with the same transport parameters and morphology, but with a modified $k_r = 10^6$ s^{-1}. One would hope that the kinetic model would provide similarly accurate fits to those shown in Figure 4 if the recombination rate alone were changed. However, this was found to not be the case. Simply reducing the recombination rate in the kinetic model to $k_r = 10^6$ s^{-1} resulted in a substantial overestimation of the MC predicted separation efficiency, as shown in the Supporting Information (Figure S5).

One could argue that this failure is due to a deficiency in the kinetic scheme of Figure 3, which in turn leads to errors when it is used more generally. Indeed, we cannot rule out this possibility. However, we note that the kinetic scheme of Figure 3 was developed with the benefit of a wide range of charge recombination data, and it was only after further testing by altering the recombination rate which showed the kinetic model was lacking in some respects. The wide range of data, and the subsequent test for robustness, was made straightforward by using a MC model and would seem to be an ideal set of conditions to derive a robust kinetic model. Hence, even though better kinetic models are possible, it is difficult to see (to these authors at least) what approach one would take to first hone alternate models to a point where it can recreate the necessary data, and second, to verify the accuracy of its predictions.

The only way in which satisfactory fits could be achieved to η (shown in Figure 5a) and dynamic behavior (Figure 6) was if all of the transport rates in the kinetic model were reduced by a

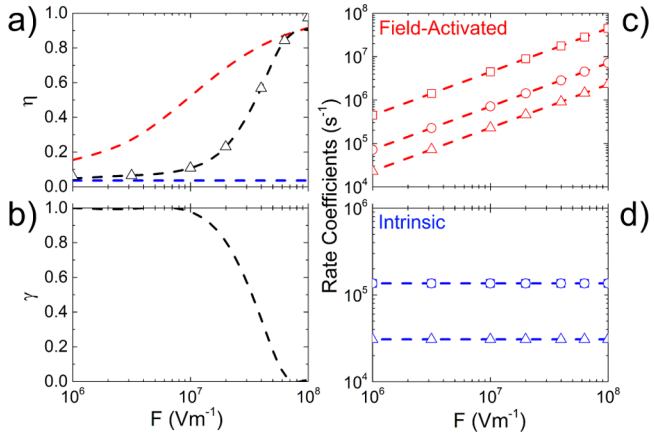

Figure 5. (a) Separation efficiencies of the field-activated (red dashed line) and intrinsic (blue dashed line) pathways alone and their combined efficiency (black dashed line), with η from the Monte Carlo simulations, assuming $k_r = 10^6$ s^{-1} (black open triangles). (b) Fraction of CT states in the intrinsic decay channel (γ) as a function of varying electric field (F). (c) and (d) show the variation of the rate coefficients k_s (squares), k_c (circles), and k_f (triangles) as a function of F for the field-activated ((c), red) and intrinsic ((d), blue) recombination pathways. Note that again $k_s^i = k_c^i$, so the two graphs are coincident.

dx.doi.org/10.1021/jp408063f | J. Phys. Chem. C 2014, 118, 85–91

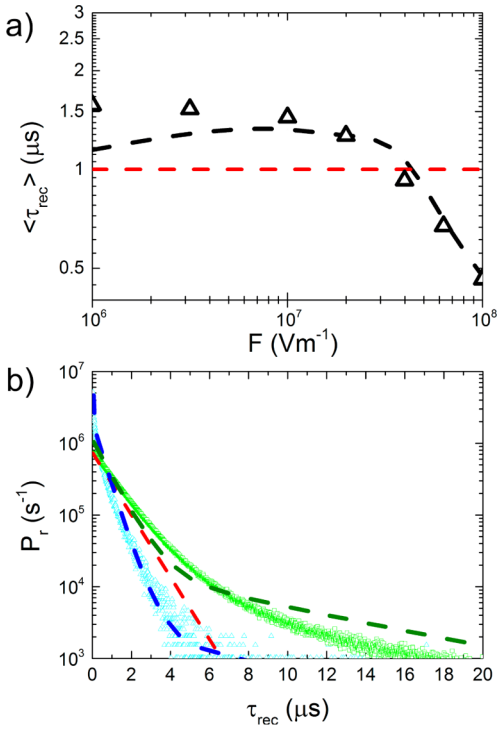

Figure 6. Recombination dynamics from Monte Carlo simulations with $k_r = 10^6$ s^{-1}. (a) $\langle\tau_{rec}\rangle$ for both the MC simulations (black triangles) and the kinetic model (black line). (b) $P_r(t)$ obtained by MC simulations (symbols) and the kinetic model (lines) for $F = 10^6$ V m^{-1} (green) and $F = 10^8$ V m^{-1} (blue). In both panels, the red dashed line shows the inverse recombination rate k_r.

factor of 10 (Figures 5c and 5d), along with some other changes to γ (Figure 5b). While this gives good fits to the MC data, we note that there is no physical justification for changing the transport rates because the transport processes in the MC model do not change. Data for all fields are included in Figure S6 of the Supporting Information.

This result is perhaps surprising. Considering first the MC data, the field-dependence of the slow decay component of $P_r(t)$ shows that this feature is related to transport and trapping processes. One might therefore expect that its importance may depend upon the relative rates of transport and recombination. However, the MC data show that this is not the case because the slow decay of $P_r(t)$ is present in the data for both $k_r = 10^7$ s^{-1} (shown in Figure 2b) and 10^6 s^{-1} (shown in Figure 6b). We attribute the insensitivity of the shape of $P_r(t)$ to the distribution of detrapping times that results from energetic disorder.[47,48] For the system examined here, hopping times spanning more than 13 orders of magnitude in time were recorded (Figure 7), meaning that some charges will inevitably be trapped for time scales similar to the $1/k_r$, irrespective of the comparatively small changes in k_r examined here. Therefore, the slow decay due to trapped charges will always be present.

Such a wide distribution of hopping times, i.e., dispersive transport, cannot be incorporated into our kinetic model. As such, in order to obtain an acceptable fit to $P_r(t)$ for the $k_r = 10^6$ s^{-1} data, more than just the recombination rate had to be changed to accommodate this deficiency. In the kinetic model, we note that the average recombination time is determined mostly by k_r and the shape of $P_r(t)$ depends upon the relationship of the recombination rate to the transport rates. With these minor changes to the fitting parameters, good

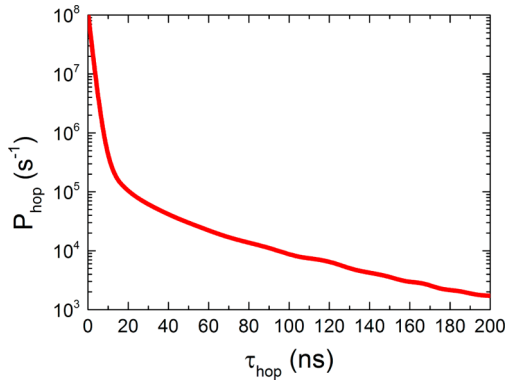

Figure 7. The probability density function for the site-to-site hopping times of charges in a fiducial simulation of $F = 10^7$ V m^{-1} and $k_r = 10^7$ s^{-1}. Although hop times covering 13 orders of magnitude are recorded, only a selection are shown here as the majority occur within 10 ns.

agreement is obtained for a variety of field-dependent dynamic data. However, we have shown that the transport rates used to obtain fits of this quality do not correspond to the actual transport processes in the MC model.

3. CONCLUSIONS

We have used Monte Carlo simulations to examine CT separation dynamics in an OPV including the effects of energetic disorder and bulk heterojunction morphology. We observed strongly biexponential decay of the recombination dynamics, similar to that shown in experiment. We argue that the slow component of $P_r(t)$ is due to trapping of charges within energetic disorder and the bulk heterojunction morphology, because increasing the electric field reduces the prominence of this feature. An alternative kinetic framework, which includes an intermediate quasi-free state between the CT and free charge states is proposed. The model is shown to fit very well the dynamic behavior of CT state recombination and separation efficiency as a function of electric field. The CT state separation behavior was examined using an altered recombination rate in the model. The present kinetic model was shown to give very poor fits to the MC data when the recombination rate was changed in the same way as the simulations. To obtain good fits to MC data, the transport rate coefficients in the kinetic model had to be altered even though the description of transport in the MC model was unchanged. This shows that kinetic models can be used to successfully fit a wide variety of data describing CT state behavior, but the derived rate does not have exact correspondence with the physical processes occurring in the OPV. We attribute this shortcoming of kinetic models to the difficulty in describing dispersive hopping transport.

■ ASSOCIATED CONTENT

Supporting Information

$P_r(t)$ for all field values, CT state lifetime data, kinetic model fits to MC data considering a single decay channel, $\langle\tau_{rec}\rangle$ data in which integration does not account for available signal-to-noise ratios, and the kinetic model fits to MC data in which the recombination rate is modified. This material is available free of charge via the Internet at http://pubs.acs.org. Access to underlying research materials: the software code used to analyze the data is copyright to Durham University subject to license by Cambridge University Enterprise; the data is held by

dx.doi.org/10.1021/jp408063f | J. Phys. Chem. C 2014, 118, 85−91

Durham University and can be accessed by contacting the corresponding author.

AUTHOR INFORMATION

Corresponding Author

*E-mail: chris.groves@durham.ac.uk.

Notes

The authors declare no competing financial interest.

ACKNOWLEDGMENTS

The authors thank Nigel Clarke for generating the morphology used in this investigation. MC simulations were performed on Durham University's High Performance Computing cluster, Hamilton. M.L.J. has a scholarship funded by EPSRC doctoral training award.

ABBREVIATIONS

OPV, organic photovoltaic; BHJ, bulk heterojunction; MC, Monte Carlo; CT, charge-transfer; QF, quasi-free; FC, free charges; GS, ground state

REFERENCES

(1) Li, Y. *Acc. Chem. Res.* **2012**, *45*, 723−733.
(2) Arias, A. C.; MacKenzie, J. D.; McCulloch, I.; Rivnay, J.; Salleo, A. *Chem. Rev.* **2010**, *110*, 3−24.
(3) Krebs, F. C.; Tromholt, T.; Jørgensen, M. *Nanoscale* **2010**, *2*, 873−886.
(4) Alvarado, S. F.; Seidler, P. F.; Lidzey, D. G.; Bradley, D. D. C. *Phys. Rev. Lett.* **1998**, *81*, 1082−1085.
(5) Onsager, L. *Phys. Rev.* **1938**, *54*, 554−557.
(6) Braun, C. L. *J. Chem. Phys.* **1984**, *80*, 4157−4161.
(7) Howard, I. A.; Mauer, R.; Meister, M.; Lacquai, F. *J. Am. Chem. Soc.* **2010**, *132*, 14866−14876.
(8) Veldman, D.; Ipek, Ö.; Meskers, S. C. J.; Sweelssen, J.; Koetse, M. M.; Veenstra, S. C.; Kroon, J. M.; van Bavel, S. S.; Loos, J.; Janssen, R. A. J. *J. Am. Chem. Soc.* **2008**, *130*, 7721−7735.
(9) Dibb, G. F. A.; Jamieson, F. C.; Maurano, A.; Nelson, J.; Durrant, J. R. *J. Phys. Chem. Lett.* **2013**, *4*, 803−808.
(10) Park, S. H.; Roy, A.; Beaupreé, S.; Cho, S.; Coates, N.; Moon, J. S.; Moses, D.; Leclerc, M.; Lee, K.; Heeger, A. J. *Nat. Photonics* **2009**, *3*, 297−303.
(11) Clarke, T. M.; Durrant, J. R. *Chem. Rev.* **2010**, *110*, 6736−6767.
(12) Borsenberger, P. M.; Ateya, A. I. *J. Appl. Phys.* **1979**, *50*, 909−913.
(13) Mihailetchi, V. D.; Koster, L. J. A.; Hummelen, J. C.; Blom, P. W. M. *Phys. Rev. Lett.* **2004**, *93*, 216601:1−216601:4.
(14) Friend, R. H.; Phillips, M.; Rao, A.; Wilson, M. W. B.; Li, Z.; McNeill, C. R. *Faraday Discuss.* **2011**, *155*, 339−348.
(15) Ohkita, H.; Cook, S.; Astuti, Y.; Duffy, W.; Tiemey, S.; Zhang, W.; Heeney, M.; McCulloch, I.; Nelson, J.; Bradley, D. D. C.; Durrant, J. R. *J. Am. Chem. Soc.* **2008**, *130*, 3030−3042.
(16) Hwang, I.-W.; Soci, C.; Moses, D.; Zhu, Z.; Waller, D.; Gaudiana, R.; Brabec, C. J.; Heeger, A. J. *Adv. Mater.* **2007**, *19*, 2307−2312.
(17) Bakulin, A. A.; Rao, A.; Pavelyev, V. G.; van Loosdrecht, P. H. M.; Pshenichnikov, M. S.; Niedzialek, D.; Cornil, J.; Beljonne, D.; Friend, R. H. *Science* **2012**, *335*, 1340−1344.
(18) Coropceanu, V.; Cornil, J.; Demetrio, A.; da Silva, F.; Olivier, Y.; Silbey, R.; Brédas, J.-L. *Chem. Rev.* **2007**, *107*, 926−952.
(19) Groves, C.; Marsh, R. A.; Greenham, N. C. *J. Chem. Phys.* **2008**, *129*, 114903:1−114903:7.
(20) van Eersel, H.; Janssen, R. A. J.; Kemerink, M. *Adv. Funct. Mater.* **2012**, *22*, 2700−2708.
(21) Gregg, B. A. *J. Phys. Chem. Lett.* **2011**, *2*, 3013−3015.
(22) McMahon, D. P.; Cheung, D. L.; Troisi, A. *J. Phys. Chem. Lett.* **2011**, *2*, 2737−2741.
(23) Groves, C. *Energy Environ. Sci.* **2013**, *6*, 1546−1551.
(24) Bakulin, A. A.; Dimitrov, S. D.; Rao, A.; Chow, P. C. Y.; Nielsen, C. B.; Schroeder, B. C.; McCulloch, I.; Bakker, H. J.; Durrant, J. R.; Friend, R. H. *J. Phys. Chem. Lett.* **2013**, *4*, 209−215.
(25) Grancini, G.; Maiuri, M.; Fazzi, D.; Petrozza, A.; Egelhaaf, H.-J.; Brida, D.; Cerullo, G.; Lanzani, G. *Nat. Mater.* **2013**, *12*, 29−33.
(26) Caruso, D.; Troisi, A. *Proc. Natl. Acad. Sci. U.S.A.* **2012**, *109*, 13498−13502.
(27) Groves, C.; Blakesley, J. C.; Greenham, N. C. *Nano Lett.* **2010**, *10*, 1063−1069.
(28) Groves, C.; Kimber, R. G. E.; Walker, A. B. *J. Chem. Phys.* **2010**, *133*, 144110:1−14410:7.
(29) Kimber, R. G. E.; Walker, A. B.; Schröder-Turk, G. E.; Cleaver, D. J. *Phys. Chem. Chem. Phys.* **2010**, *12*, 844−851.
(30) Yan, H.; Swaraj, S.; Wang, C.; Hwang, I.; Greenham, N. C.; Groves, C.; Ade, H.; McNeill, C. R. *Adv. Funct. Mater.* **2010**, *20*, 4329−4337.
(31) Kimber, R. G. E.; Wright, E. N.; O'Kane, S. E. J.; Walker, A. B.; C, B. J. *Phys. Rev. B* **2012**, *86*, 235206:1−235206:9.
(32) Lyons, B. P.; Clarke, N.; Groves, C. *Energy Environ. Sci.* **2012**, *5*, 7657−7663.
(33) Hederson, I. C.; Clarke, N. *Macromol. Theory Simul.* **2005**, *14*, 435−443.
(34) Fukuda, J.; Yoneya, M.; Yokoyama, H. *Phys. Rev. E* **2006**, *73*, 066706:1−066706:9.
(35) Blakesley, J. C.; Clubb, H. S.; Greenham, N. C. *Phys. Rev. B* **2010**, *81*, 045210:1−045210:9.
(36) Marcus, R. A. *Annu. Rev. Phys. Chem.* **1964**, *15*, 155−196.
(37) Westenhoff, S.; Howard, I. A.; Hodgkiss, J. M.; Kirov, K. R.; Bronstein, H. A.; Williams, C. K.; Greenham, N. C.; Friend, R. H. *J. Am. Chem. Soc.* **2008**, *130*, 13653−13658.
(38) Massip, S.; Oberhumer, P. M.; Tu, G.; Albert-Seifried, S.; Huck, W. T. S.; Friend, R. H.; Greenham, N. C. *J. Phys. Chem. C* **2011**, *115*, 25046−25055.
(39) Hodgkiss, J. M.; Campbell, A. R.; Marsh, R. A.; Rao, A.; Albert-Seifried, S.; Friend, R. H. *Phys. Rev. Lett.* **2010**, *104*, 177701:1−177701:4.
(40) Pensack, R. D.; Banyas, K. M.; Barbour, L. W.; Hegadorn, M.; Asbury, J. B. *Phys. Chem. Chem. Phys.* **2009**, *11*, 2575−2591.
(41) Tong, M.; Coates, N. E.; Moses, D.; Heeger, A. J. *Phys. Rev. B* **2010**, *81*, 125210:1−125210:6.
(42) Soon, Y. W.; Clarke, T. M.; Zhang, W.; Agostinelli, T.; Kirkpatrick, J.; Dyer-Smith, C.; McCulloch, I.; Nelson, J.; Durrant, J. R. *Chem. Sci.* **2011**, *2*, 1111−1120.
(43) Howard, I. A.; Laquai, F. *Macromol. Chem. Phys.* **2010**, *211*, 2063−2070.
(44) Guo, J.; Liang, Y.; Xiao, S.; Szarko, J. M.; Sprung, M.; Mukhopadhyay, M. K.; Wang, J.; Yu, L.; Chen, L. X. *New J. Chem.* **2009**, *33*, 1497−1507.
(45) Wojcik, M.; Tachiya, M. *J. Chem. Phys.* **2009**, *130*, 104107:1−104107:9.
(46) Yan, H.; Swaraj, S.; Wang, C.; Hwang, I.; Greenham, N. C.; Groves, C.; Ade, H.; McNeill, C. R. *Adv. Funct. Mater.* **2010**, *20*, 4329−4337.
(47) Scher, H.; Montroll, E. W. *Phys. Rev. B* **1975**, *12*, 2455−2477.
(48) Khan, R. U. A.; Poplavskyy, D.; Kreouzis, T.; Bradley, D. D. C. *Phys. Rev. B* **2007**, *75*, 035215:1−035215:14.